Search for Point-Like Sources of Cosmic Rays with Energies above $10^{18.5}$ eV in the HiRes–I Monocular Data-Set

R.U. Abbasi [a], T. Abu-Zayyad [a], J.F. Amann [b], G. Archbold [a], R. Atkins [a], J.A. Bellido [c], K. Belov [a], J.W. Belz [d], S. BenZvi [h], D.R. Bergman [e], G.W. Burt [a], Z. Cao [a], R.W. Clay [c], B.M. Connolly [h], B.R. Dawson [c], W. Deng [a], Y. Fedorova [a], J. Findlay [a], C.B. Finley [h], W.F. Hanlon [a], C.M. Hoffman [b], M.H. Holzscheiter [b], G.A. Hughes [e], P. Hüntemeyer [a], C.C.H. Jui [a], K. Kim [a], M.A. Kirn [d,*], E.C. Loh [a], M.M. Maestas [a], N. Manago [f], L.J. Marek [b], K. Martens [a], J.A.J. Matthews [g], J.N. Matthews [a], A. O'Neill [h], C.A. Painter [b], L. Perera [e], K. Reil [a], R. Riehle [a], M.D. Roberts [g], M. Sasaki [f], S.R. Schnetzer [e], K.M. Simpson [c], G. Sinnis [b], J.D. Smith [a], R. Snow [a], P. Sokolsky [a], C. Song [h], R.W. Springer [a], B.T. Stokes [a], J.R. Thomas [a], S.B. Thomas [a], G.B. Thomson [e], D. Tupa [b], S. Westerhoff [h], L.R. Wiencke [a], A. Zech [e]

The High–Resolution Fly's Eye Collaboration

[a] *University of Utah, Department of Physics and High Energy Astrophysics Institute, Salt Lake City, Utah, USA*

[b] *Los Alamos National Laboratory, Los Alamos, NM, USA*

[c] *University of Adelaide, Department of Physics, Adelaide, South Australia*

[d] *University of Montana, Department of Physics and Astronomy, Missoula, Montana, USA.*

[e] *Rutgers — The State University of New Jersey, Department of Physics and Astronomy, Piscataway, New Jersey, USA*

[f] *University of Tokyo, Institute for Cosmic Ray Research, Kashiwa, Japan*

[g] *University of New Mexico, Department of Physics and Astronomy, Albuquerque, New Mexico, USA*

[h] *Columbia University, Department of Physics and Nevis Laboratory, New York, New York, USA*

Abstract

We report the results of a search for point-like deviations from isotropy in the arrival directions of ultra–high energy cosmic rays in the northern hemisphere. In the monocular data set collected by the High–Resolution Fly's Eye, consisting of 1,525 events with energy exceeding $10^{18.5}$ eV, we find no evidence for point-like excesses. We place 90% c.l. upper limits less than or equal to 0.8 cosmic rays/km^{2}yr on the flux from such sources as a function of position in the sky.

Key words: cosmic rays, anisotropy, point source, HiRes

1   Introduction

In the search for the origins of ultra–high energy cosmic rays (UHECR), a variety of strategies have been employed to detect deviations from isotropy in event arrival directions. The results of these searches have been ambiguous. The most recent results [1] have supported the null hypothesis for large–scale dipole behavior in arrival directions for particles above $10^{18.5}$ eV. However, previous experiments [2] have found evidence for a dipole moment in Right Ascension (RA) at energies above 10^{18} eV. On smaller angular scales, excesses have been alternately claimed and refuted in the vicinity of Cygnus X-3 [3,4,5,6], an x-ray binary within our galaxy, including the report of a possible excess in a point-source search [7].

Point-like excesses at these energies can arise from only a limited number of source scenarios. Galactic and extragalactic magnetic fields are expected to produce large perturbations in the arrival directions of charged particles: A proton of energy $10^{18.5}$ eV may be deflected by several tens of degrees as it traverses the disk of the Milky Way galaxy, with a typical magnetic field of order 1 microgauss [8]. A compact arrival direction excess at these energies would therefore suggest neutral primaries. Neutrons however possess a lifetime of 3×10^{12} seconds at $10^{18.5}$ eV, and therefore cannot have originated more than 30 kpc from Earth. Thus any viable source of standard model neutral hadronic matter would have to be located within the Milky Way Galaxy.

In this paper, we conduct a search for point-like behavior in arrival direction of cosmic ray events above $10^{18.5}$ eV in the northern hemisphere, using a skymap technique in which we evaluate our sensitivity using Monte Carlo simulated

* Corresponding author. *E-mail Address*: mkirn@physics.montana.edu

sources. In addition, we consider the historically significant source candidate Cygnus X-3 as the focus of an *a priori* search.

2   The HiRes Monocular Data Set

The High–Resolution Fly's Eye (HiRes) consists of two nitrogen fluorescence observatories — HiRes–I and HiRes–II — separated by 12.6 km and located at Dugway, Utah. HiRes was conceived as a stereo detector, however due to the larger available statistics it is desirable to reconstruct extensive airshowers in monocular mode as well. This HiRes–I monocular data set consists of 2,820 good–weather detector hours of data, collected between May 1997 and February 2003. A total of 1,525 events with energies exceeding $10^{18.5}$ eV were collected during this time and are included in the present analysis.

The HiRes-I monocular data set and airshower reconstruction by profile constrained fitting has recently been described in the literature [9]. A residual effect of the profile–constrainted fit technique is orientation–dependent (elliptical) uncertainties in the airshower arrival directions. In Figure 1, the airshower reconstruction geometry is illustrated for a monocular air fluorescence detector. In this view, the shower–detector plane (SDP) for HiRes–I events is well–reconstructed, with uncertainty parameterized as

$$\sigma_{SDP} = 88.151° e^{-.51\Delta\chi} + 0.374° \tag{1}$$

where $\Delta\chi$ is the angular tracklength of the shower in degrees. Typical values of σ_{SDP} for this analysis range from $0.4° \rightarrow 1.7°$. The angle of the track within the SDP, Ψ, is less well reconstructed and is parameterized by

$$\sigma_{\Psi} = 18.381° e^{-\log_{10}(1.45E)} + 4.073° \tag{2}$$

where the energy E is expressed in EeV (10^{18} eV). Typical values of σ_{Ψ} in this analysis range from $5.4° \rightarrow 15°$.

In Figure 2, we plot the skymap formed from the arrival directions of events in the present data set. Each event's "error ellipse" is represented by generating 1,000 points per event, distributed according to the Gaussian error model of Equations 1 and 2. Figure 2 is plotted in equatorial coordinates as a polar plot. Note that bins are assigned using a cartesian projection of the polar plot shown in Figure 2 and all similar figures. As such, angular bin size varies across the map, but averages approximately $1° \times 1°$.

We next discuss the Monte Carlo technique by which we evaluate the significance of fluctuations in the skymap as well as our sensitivity to point-like
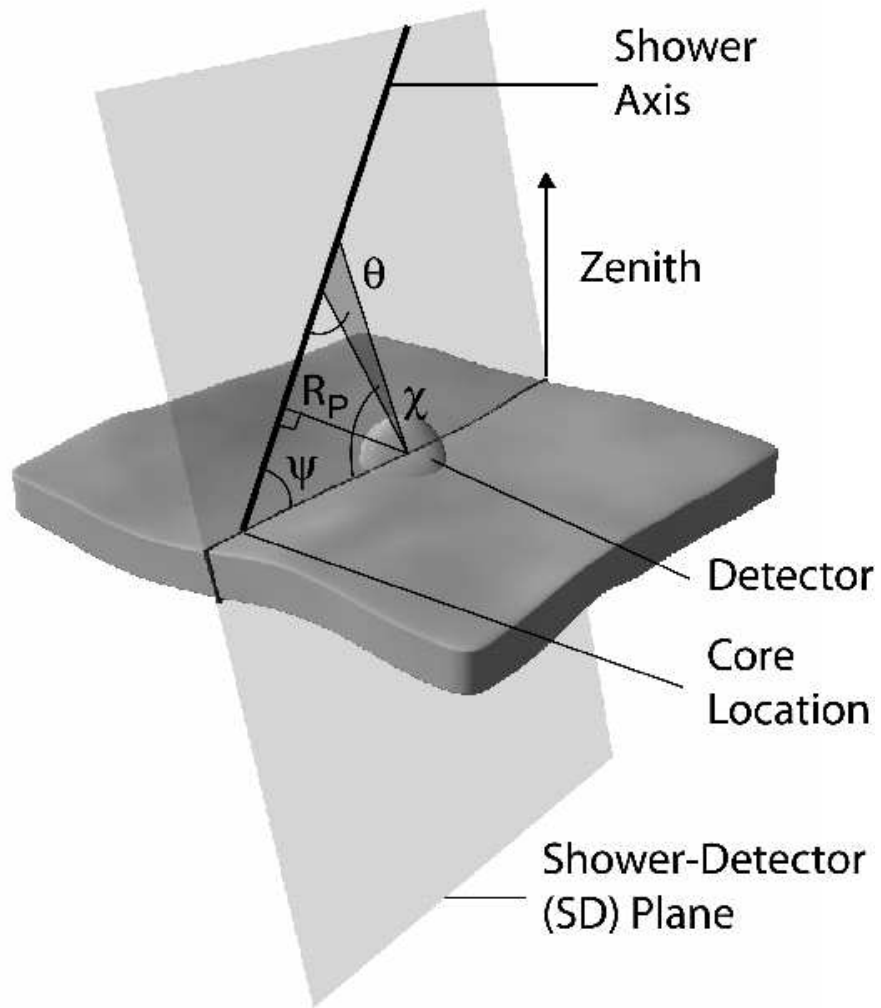
Fig. 1. The geometry of reconstruction for a monocular air fluorescence detector.
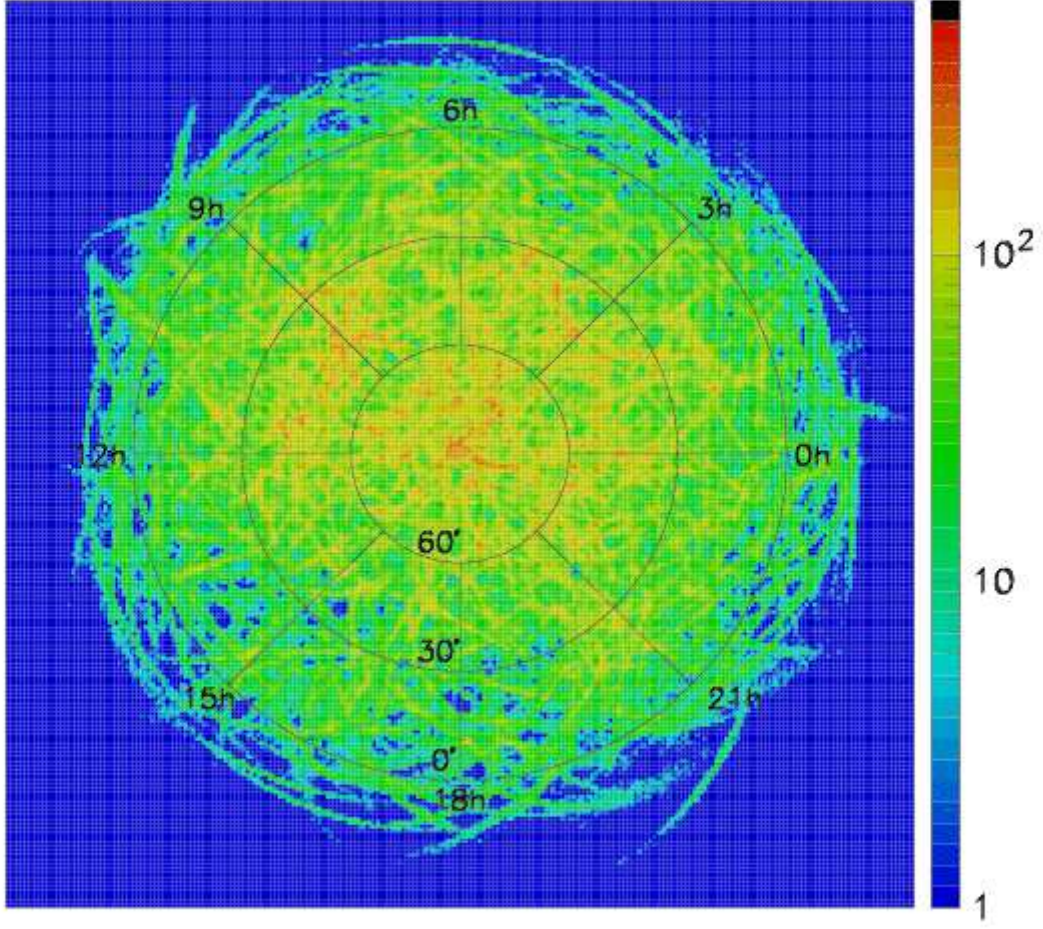behavior in arrival direction.

Fig. 2. Skymap of arrival directions of events in the the HiRes–I monocular data set, plotted in polar projection, equatorial coordinates. Each HiRes event is represented by 1,000 points randomly thrown according to the elliptical Gaussian error model of Equations 1 and 2. The bin size in this plot (and all similar plots) is approximately $1° \times 1°$.

3   The Monte Carlo; Comparison of Data to Expectation from an Isotropic Background

We use a library of simulated events, generated by the Monte Carlo technique and reconstructed using the profile–constrained reconstruction program to determine the background expectation for isotropically distributed sources as well as to evaluate our sensitivity to point-like behavior in arrival direction. For this library, an isotropic distribution is assumed for events possessing the spectrum and composition reported by the stereo Fly's Eye experiment [10,11].

A detector runtime database is used to randomly assign a time from detector "on" periods to each event in the isotropic background data set. A total of 1,000 isotropic data sets with the same sky exposure as the HiRes–I monocular data set were generated for comparison studies. Further discussion of this Monte Carlo can be found in Reference [1]. In Figures 3 and 4 we compare the data and Monte Carlo distributions of events in the variables RA and DEC, respectively.
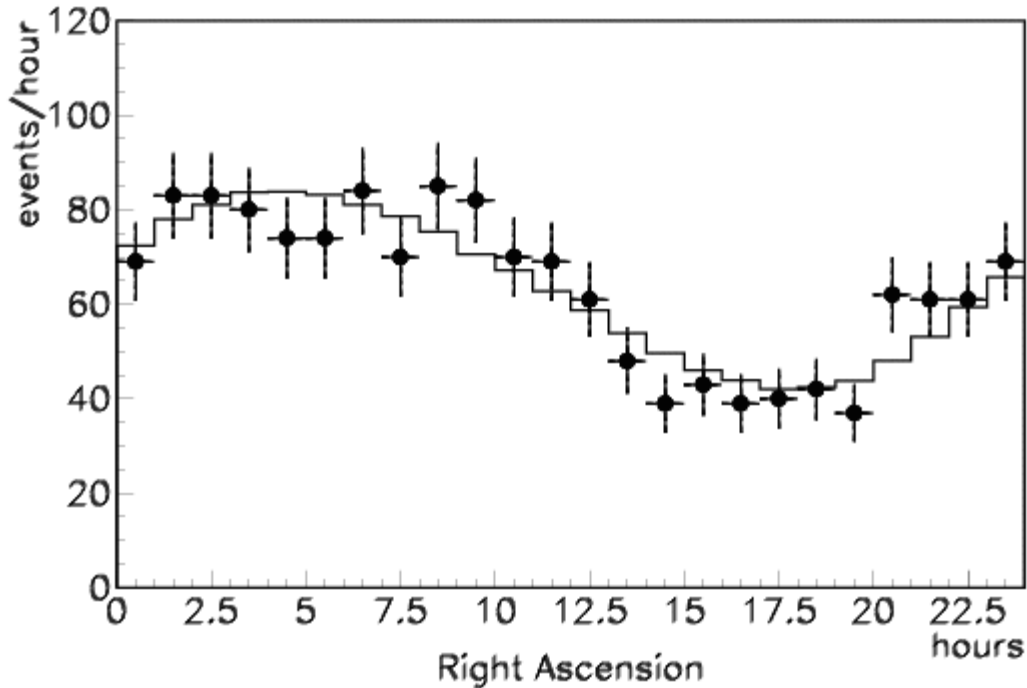

Fig. 3.   Comparison of HiRes–I data (points) and Monte Carlo (solid histogram) distributions in right ascension (RA).

In order to understand the significance of the fluctuations in Figure 2, we compare the data on a bin-by-bin basis to the 1,000 simulated data sets. Defining N_{DATA} as the bin density of the data, N_{MC} as the bin density of the
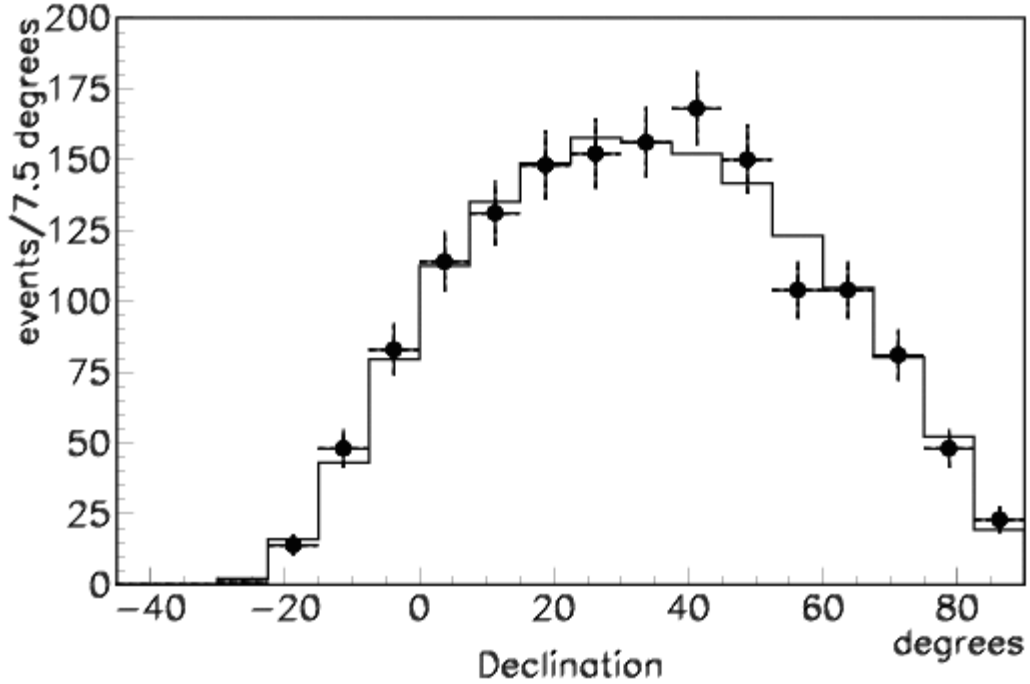
6

Fig. 4. Comparison of HiRes–I data (points) and Monte Carlo (solid histogram) distributions in declination (DEC).

simulated isotropic data sets, and σ_{MC} as the standard deviation of the Monte Carlo bin density, the variable

$$\chi_1 = \frac{(N_{DATA} - \langle N_{MC}\rangle)}{\sigma_{MC}} \tag{3}$$

provides a measure of the fluctuation per bin. Figure 5 shows the distribution of χ_1 as a function of position in the sky for the HiRes–I monocular data set as extracted from this technique.

The bin-by-bin distributions of χ_1 are non-Gaussian (Figure 6) and vary as a function of position in the sky. Thus it is necessary to develop a technique to evaluate the significance of possible sources. Our technique uses the χ_1 information in neighboring bins to pick out significant fluctuations above background from the skymap. The parameters in the technique are tuned on simulated point-like sources.
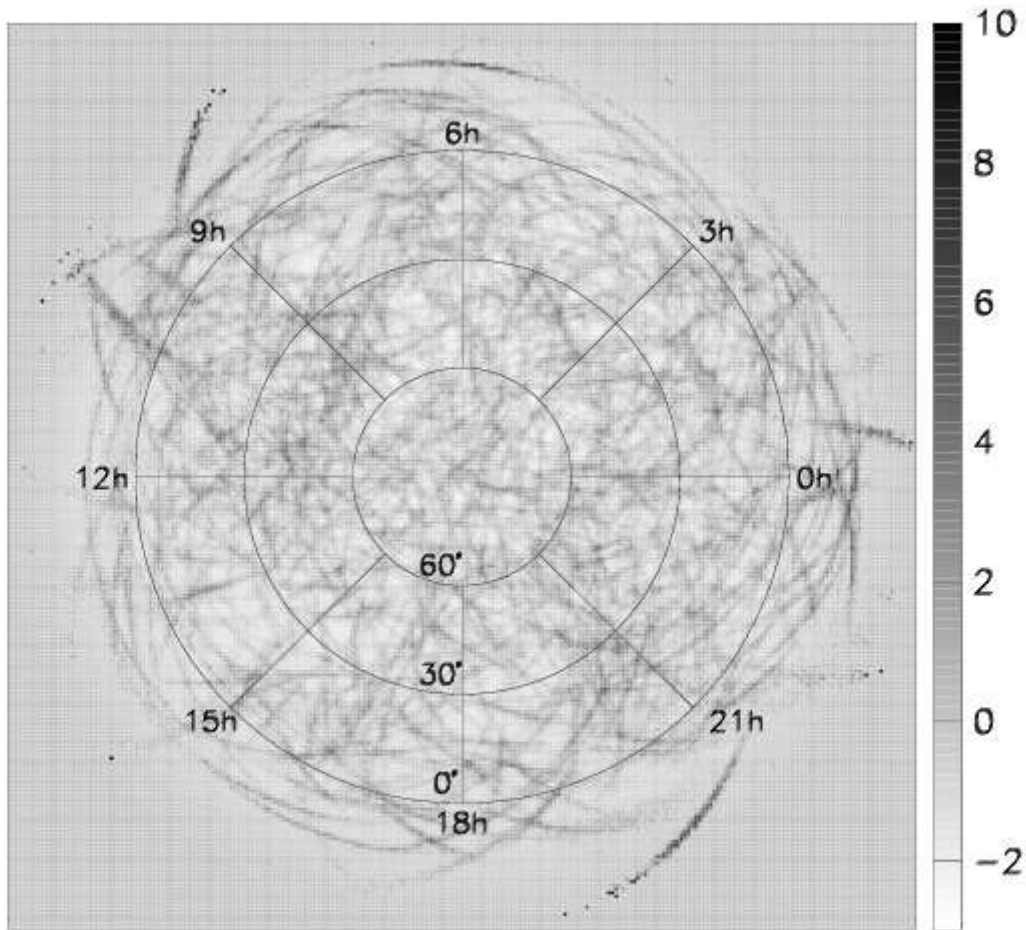
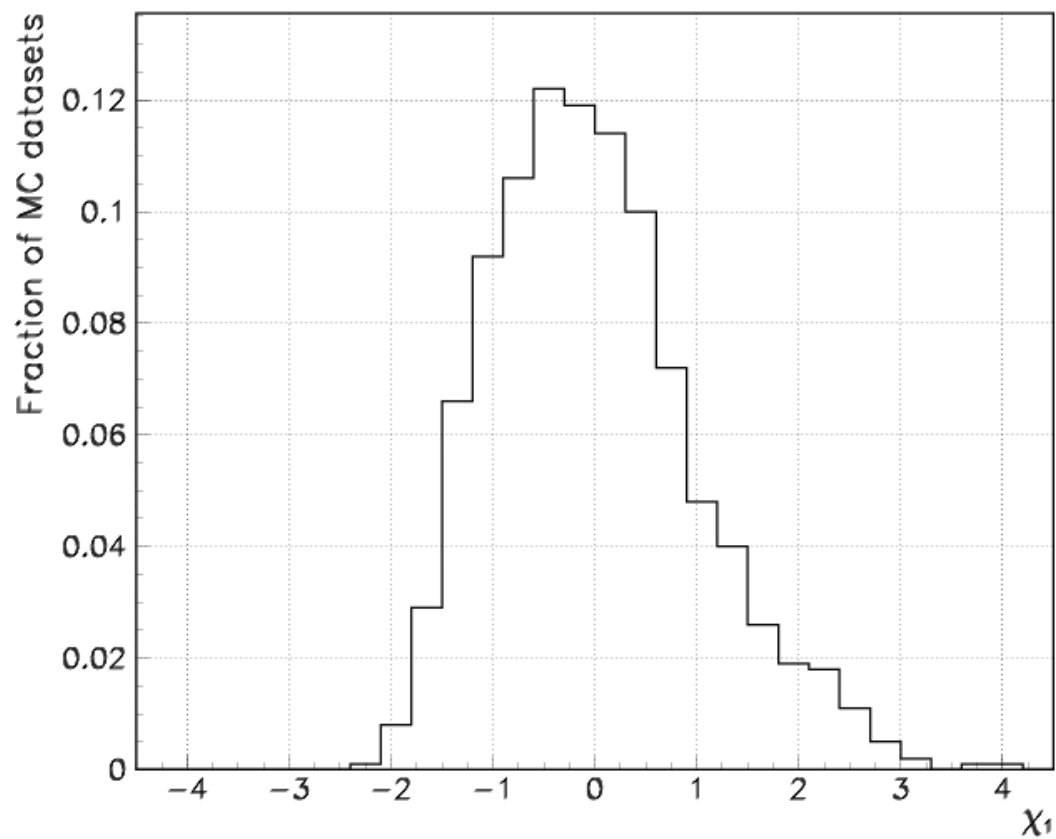Fig. 5. χ_1 (Equation 3) distribution for the HiRes-I monocular data set.

Fig. 6. Example distribution of χ_1 (Equation 3) values for 1,000 MC data sets in the bin located at 5 hours RA, 40° DEC.

4 The Monte Carlo; Simulation of Point-Like Sources

We have two objectives in simulating point-like sources: The first is using these simulated sources to tune point source selection criteria. Secondly, simulated sources provide a straighforward method by which to quantify our sensitivity to point-sources and derive flux upper limits.

Simulated source skymaps are created by randomly replacing events in a simulated isotropic data set with N_S events at the chosen position for the source. The central-value coordinates of the simulated source event are randomly shifted according to the error ellipse, which is taken from the replaced event. The shift simulates the effect of detector resolution only. Finally, the orientations of error ellipses are randomized.

An example of a simulated source is shown in Figure 7. This source is superimposed on a Monte Carlo data set in Figure 8, and the quantity χ_1 (Equation 3) is evaluated for each bin in Figure 9. We note that source events overlap in a fairly small angular region, as seen in Figure 7. Thus we have sensitivity to fairly compact deviations from isotropy, in spite of our elongated error ellipses.
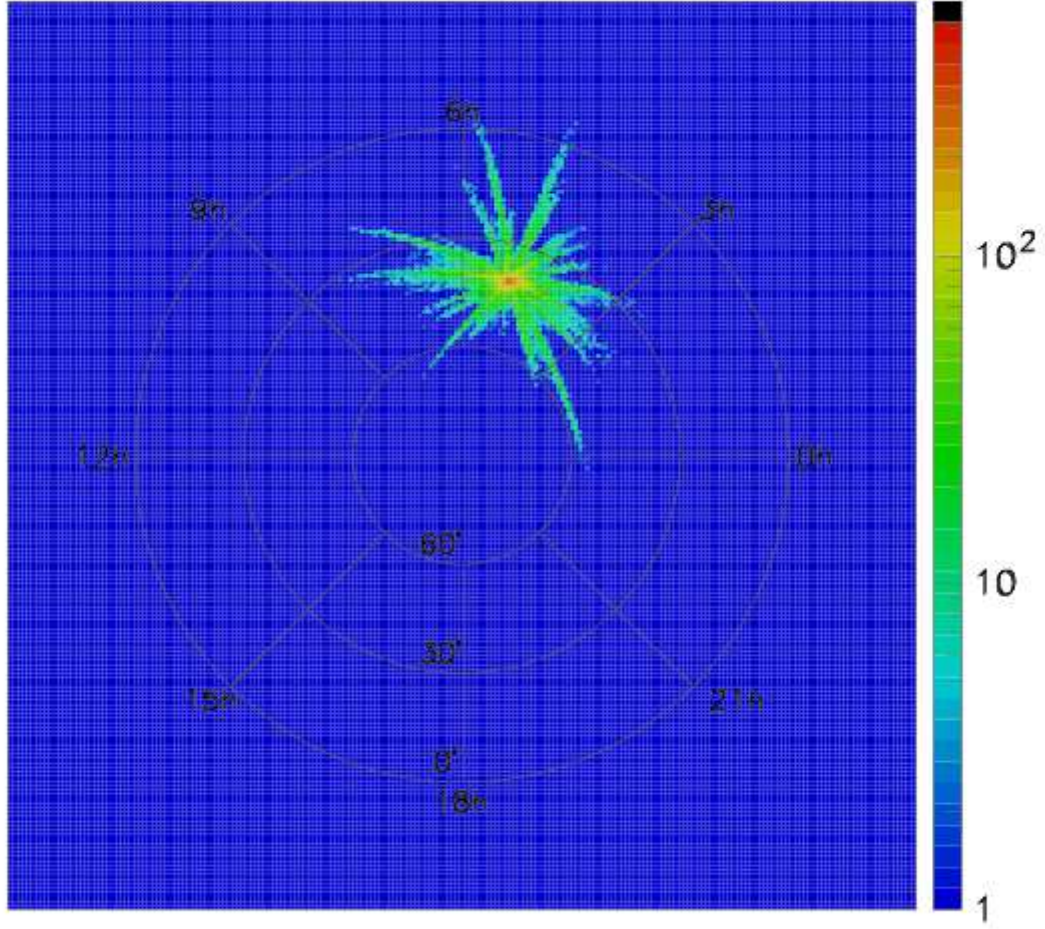
Fig. 7. An $N_S = 25$ event source shown without the isotropic background. The source has been inserted at 5 hours RA, 40° DEC. Each source event is represented by 1,000 points randomly thrown according to the elliptical Gaussian error model of Equations 1 and 2, where the error ellipse is taken from the replaced isotropic event.
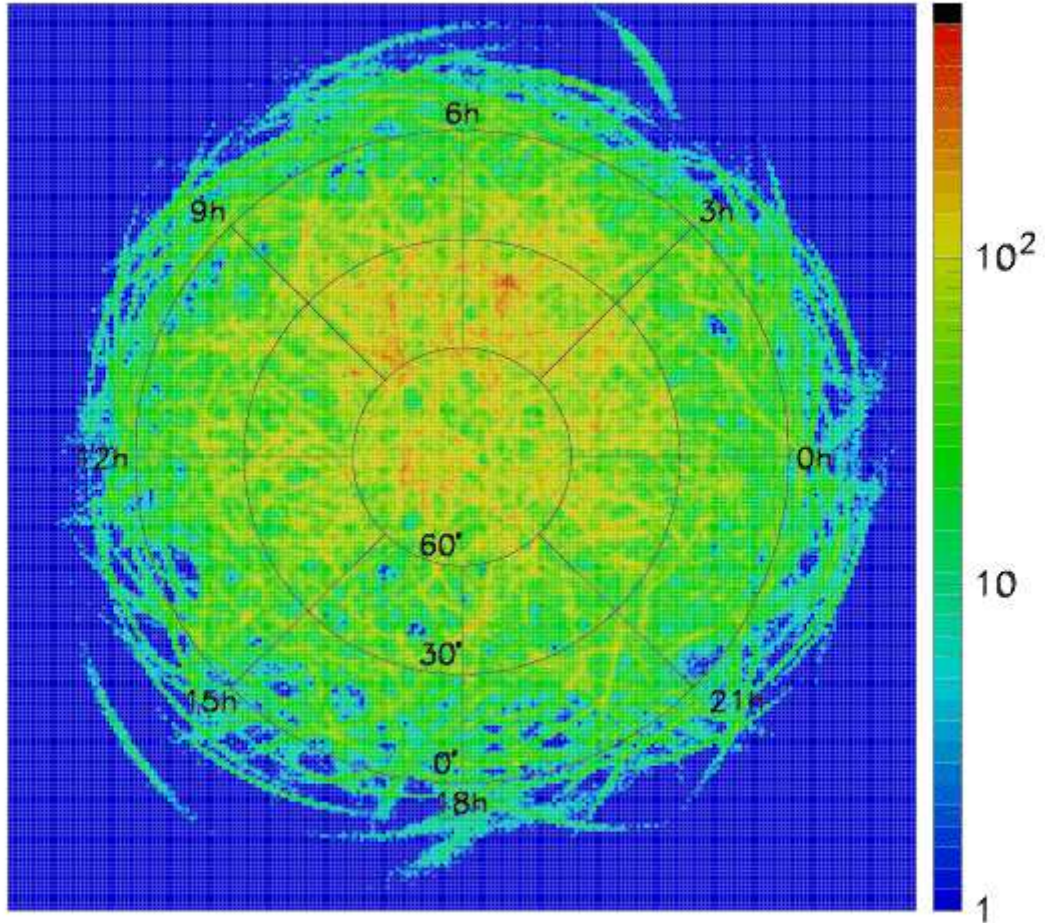
Fig. 8. Skymap of arrival directions of events for a simulated data set, having the same overall exposure as the HiRes–I monocular data set, with a 25 event source superimposed at 5 hours RA, 40° DEC (compare to Figure 2).
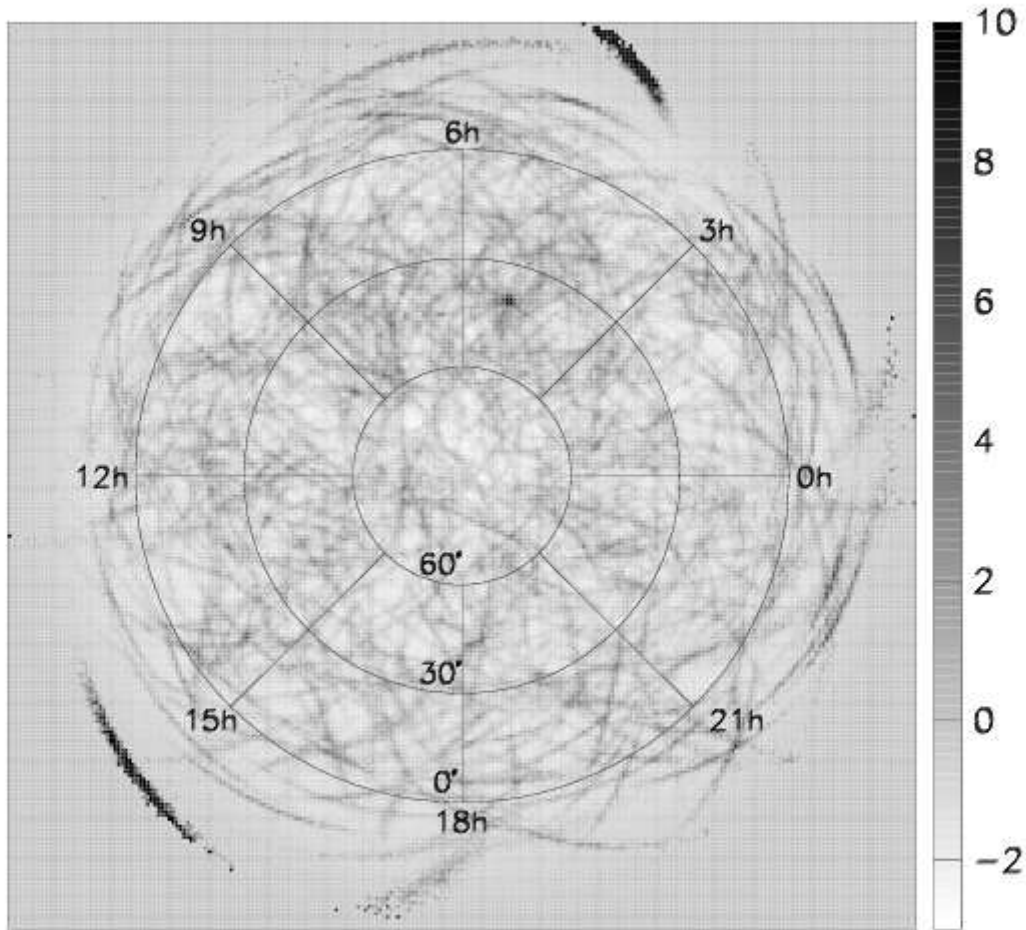
Fig. 9. χ_1 (Equation 3) for $N_S = 25$ event source inserted in an simulated isotropic data set. The source has been inserted at 5 hours RA, 40° DEC.

5 Calculation of Significances

We now describe a procedure by which we can identify point-like behavior in arrival direction (for example, the simulated source of Figures 7, 8, and 9) while simultaneously rejecting false positives arising from fluctuations of the background.

Due to detector resolution, it is desirable that we search for sources by considering points over an extended angular region. We consider a "search circle" of radius R, where R is expressed as an angle in degrees. Within the search circle, we count the fraction of bins F having a χ_1 value greater than some threshold χ_{THR}. The parameters R and χ_{THR} are chosen to optimize the signal size, and a cut is chosen on the fraction F which reduces the false positive probability to an acceptable level.

Our maximum sensitivity to point-like behavior in arrival direction, given the HiRes–I pointing uncertainty, was determined to require a search circle of $R = 2.5°$, and a value $\chi_{THR} = 4$. (In the case in which the bin densities are normally distributed, this corresponds to 4σ.) The optimum values for these parameters were determined by simulating sources at various locations in the sky and maximizing our sensitivity to these sources. The values for these parameters are found to be largely insensitive to the position in the sky and the number of events in the source. Additionally, small variations in either of these parameters do not have a significant impact on our results.

Due to low statistics at the edge of HiRes' acceptance, we consider only search circles with centers whose declinations are greater than 0°. That is, we only search for sources north of the celestial equator. Approximately 10% of HiRes events have central-value coordinates south of the equator. These events can contribute to the search if their error ellipses extend north of DEC $= -2.5°$.

In Figure 10, we have plotted for each bin the fraction F, for $R = 2.5°$ and $\chi_{THR} = 4$, of the simulated point source of Figure 8. The simulated source stands out clearly in this figure.

The final parameter in this search algorithm is the cut placed on the quantity F. We evaluate this cut by requiring that the probability of a simulated isotropic data set – *without* a superimposed simulated source — exceeding the cut be no more than 10% over the entire sky (Figure 11). We choose a cut value of $F = 0.33$, corresponding to a false–positive probability of 10%.

Figure 12 shows the F distribution for the monocular data set. The "hottest" spot on this graph, near DEC $= 20°$ and RA $= 20$ hours, has a value $F = 0.15$. 87% of simulated isotropic data sets have $F \geq 0.15$ (see Figure 11). We conclude that our observation is consistent with a fluctuation from an isotropic
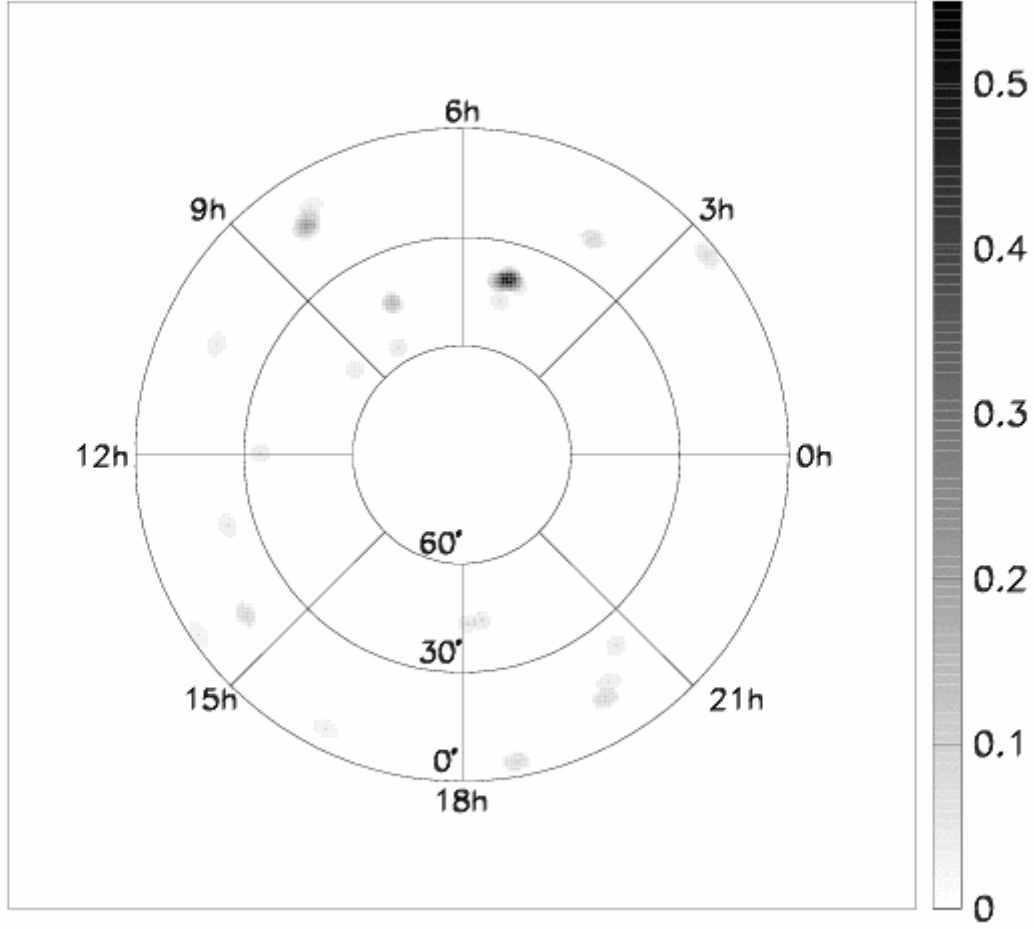
Fig. 10. F distribution derived from the χ_1 map of Figure 9. F is the fraction of bins within radius $R = 2.5°$ having a χ_1 value of 4 or greater. The simulated source at 5 hours RA, 40° DEC clearly stands out as having an exceptionally large excess fraction F.

background.

Next, we evaluate the corresponding sensitivity and flux upper limits as a function of position in the sky.
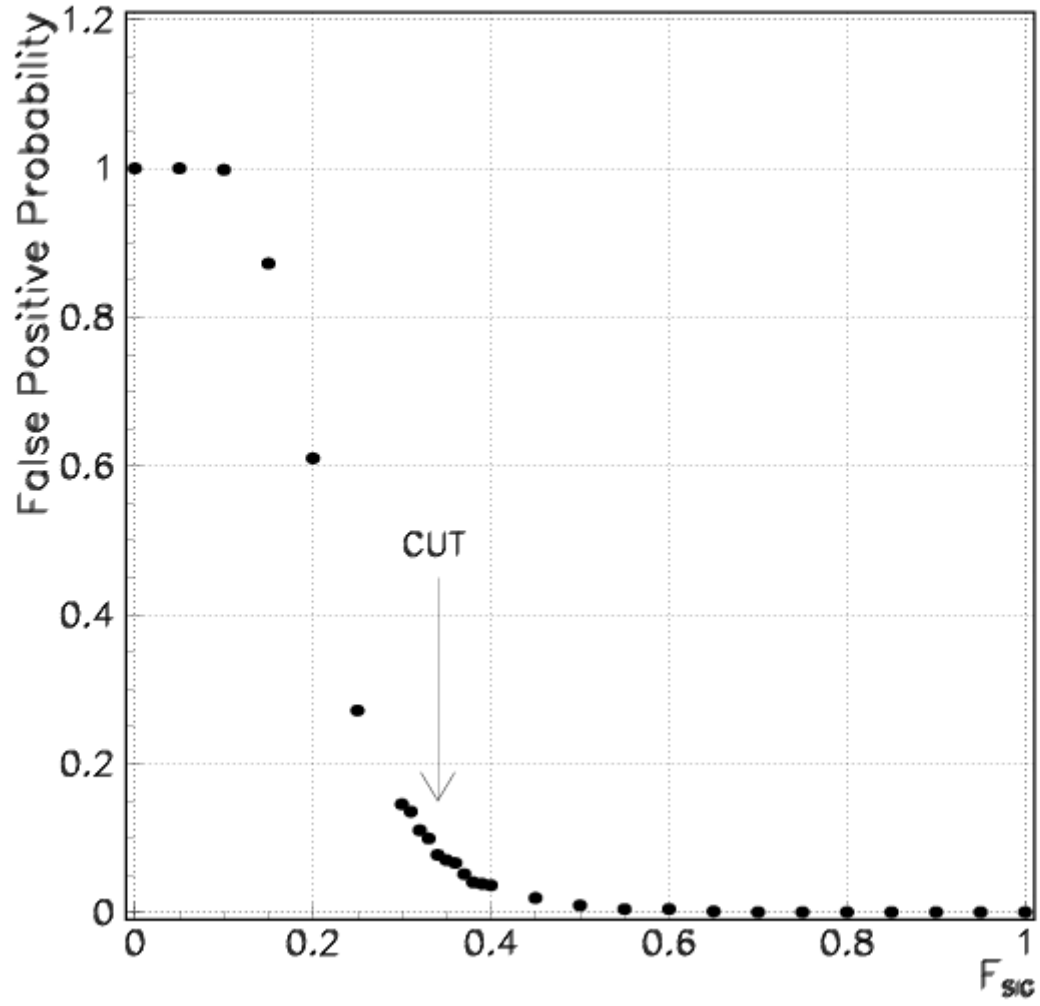
Fig. 11. Occurrence rate of false positives versus F, for a 2.5° search circle and χ_1 threshold of 4. A cut at $F = 0.33$ corresponds to a false-positive probability of 10%.
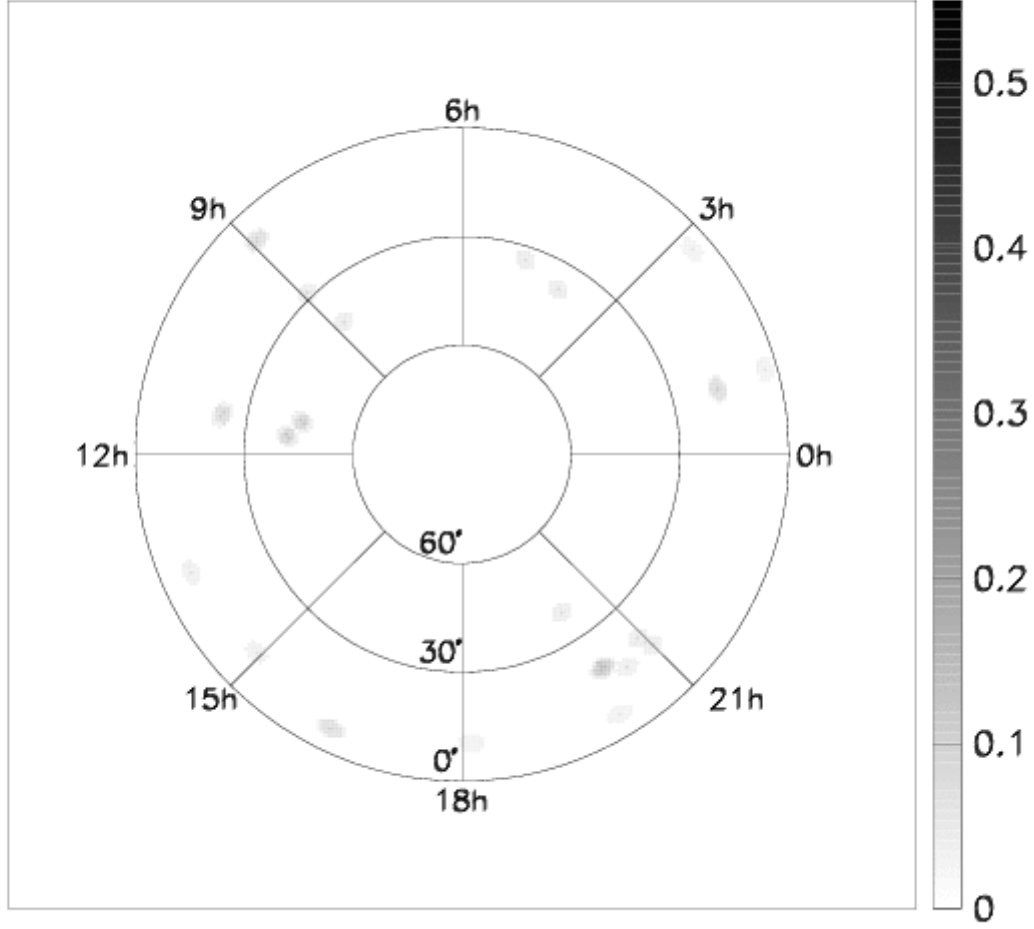
Fig. 12. F distribution derived from the HiRes–I monocular data (Figures 2 and 5). F is the fraction of bins within radius $R = 2.5°$ having a χ_1 value of 4 or greater. No points satisfy our search criteria. The largest F occurs at DEC = 20° and RA = 20 hours and has a value $F = 0.15$, corresponding to a false-positive probability of 87%.

6 Sensitivity and Upper Limits

In the preceding section, we found no evidence for the presence of point-like excesses in the HiRes–I monocular dataset above $10^{18.5}$ eV. Further, the significance of the largest point-like fluctuation in the data is well below the threshold established to minimize the likelihood of false positives in an isotropic distribution. To quantify our null result, we follow the suggestion of Feldman and Cousins [12] and calculate both a set of flux upper limits and the "sensitivity" of the experiment to such point-like excesses. The results of these calculations are reported below.

6.1 Sensitivity

The sensitivity of the experiment is defined as the average 90% confidence level flux upper limit that would be reported by an ensemble of like experiments with no true signal. Since this average upper limit will vary as a function of position on the skymap due to different background expectations, we calculate our sensitivity at set of gridpoints (Table 1) distributed evenly across the Northern Hemisphere. We choose the right ascension values of our gridpoints to correspond approximately to the HiRes "solstices" and "equinoxes", *i.e.* to the RA lines of high/low and midrange event statistics.

To determine our sensitivity to a number of "source" events $\langle N_S \rangle$ at a given gridpoint, we generate 400 simulated isotropic datasets with point-like sources superimposed. The number of events in each source is Poisson distributed with mean value $\langle N_S \rangle$. These datasets contain the same total number of events as the HiRes-I data.

We then determine the percentage of trials at each location for which our reconstruction algorithm "finds" a source of size $\langle N_S \rangle$. In the case of the sensitivity calculation, we say the algorithm "finds" a source if at one point on the skymap F fluctuates above our preselected threshold value of $F = 0.33$. The value of $\langle N_S \rangle$ for which signal was declared for 90% or better of the trials was termed $N_{.33}$.

The distribution of $N_{.33}$ at our grid points is illustrated in Figure 13. We estimate that the systematic uncertainty in the calculation of $N_{.33}$, due to uncertainties in the size of the error ellipses, is ≤ 1 event.

The HiRes-I detector flux sensitivity at each grid point is $N_{.33}$ at that point divided by the local exposure. We calculate the detector exposure [13] for point sources at the grid points by the following procedure: Monte Carlo events are generated at the grid points, assigned a time from the distribution of HiRes
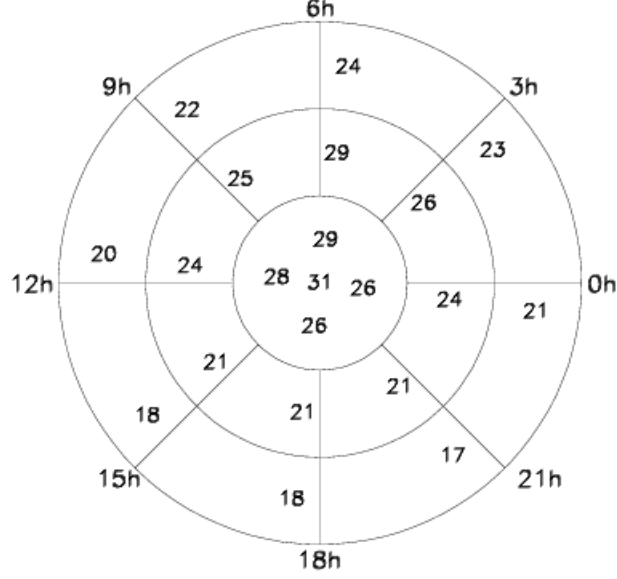
Fig. 13. Numerical values of $N_{.33}$ — the mean number of source events for which signal was declared in 90% or better of 400 trials with a cut on F of .33 — at 21 grid points in the Northern Hemisphere. Exact numbers and locations of gridpoints are given in Table 1. The systematic uncertainty in the calculation of $N_{.33}$, due to uncertainties in the size of the error ellipses, is ≤ 1 event.

detector ontimes, and projected towards the detector aperture. Local coordinates and times are determined, then the event is paired with a shower from the Monte Carlo event library having similar local coordinates. An attempt is then made to reconstruct the Monte Carlo event with the profile–constrained fitting technique. The exposure, defined as the fraction of events reconstructed multiplied by the detector aperture (area) and time, can then be used to determine flux sensitivity (as well as flux upper limits) for each of the grid locations. These exposures are listed in Table 1. The final flux sensitivities are shown in Table 1 and Figure 14.
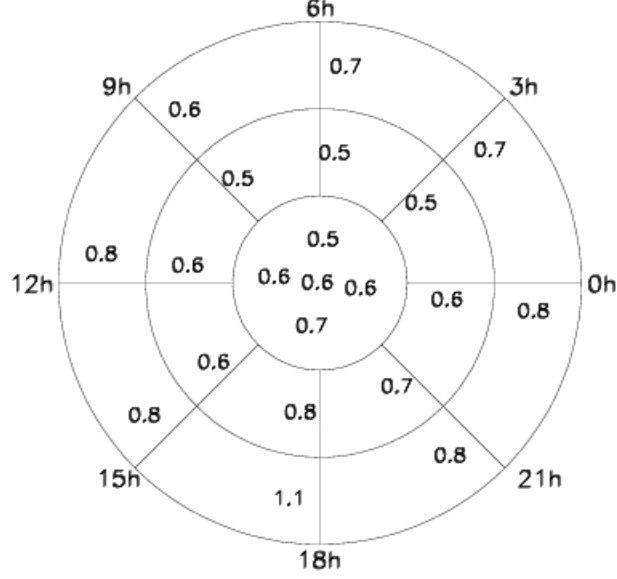
19

Fig. 14. Flux sensitivity (cosmic rays/km^{2}yr) at 21 grid points in the Northern Hemisphere. Sensitivity is calculated by dividing $N_{.33}$ (Figure 13) by the exposure at each grid point. The numbers along with the exact locations of grid points are given in Table 1.

6.2   Upper Limits

We place our 90% confidence level flux upper limits by making use of the fact that F never fluctuated above 0.15 in the HiRes-I data. (Figure 10. We determine the value of $N_{.15}$ — the mean number of source events for which signal was declared in 90% or better of trials with a threshold of $F = .15$ — in the same manner in which we determined $N_{.33}$ in the previous section. he results are summarized in Figure 15. Our 90% c.l. flux upper limit at each grid point (Figure 16) is $N_{.15}$ at that point divided by the local exposure. The largest flux upper limit across the entire sky is 0.8 cosmic rays above $10^{18.5}$eV per km^{2}yr.

Finally, we note that the *a priori* source candidate in the direction of Cygnus X-3 (RA 20.5 hours, DEC 40.7°) is very near the grid point located at RA 20.5 hours, DEC 45°. We place a 90% c.l. flux upper limit from Cygnus X-3 at

20

0.5 cosmic rays above $10^{18.5}$eV per km^{2}yr. Previous Cygnus X–3 flux results were drawn from events samples with energies above 5×10^{17} eV, so a direct comparison is impossible. We can infer — assuming that any cosmic rays from Cygnus X-3 have an energy spectrum similar to that of the full sky — that an extrapolation of our result is not competitive with prior upper limits for events above 5×10^{17} eV. However, this is the first reported measurement for a high-statistics sample above $10^{18.5}$eV.
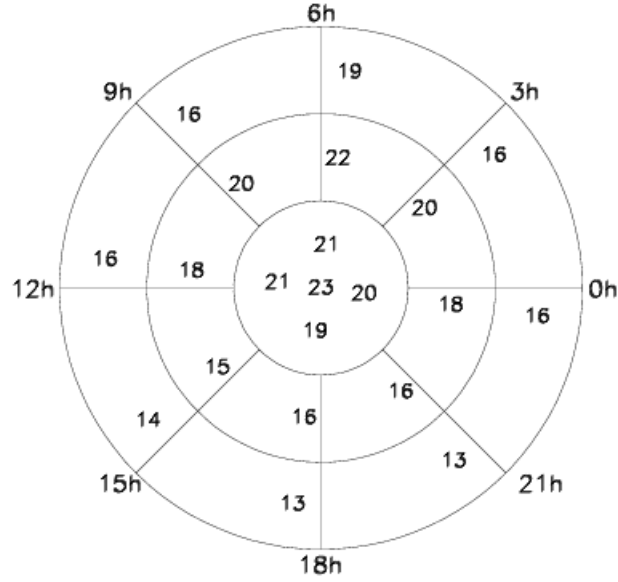

Fig. 15. Numerical values of $N_{.15}$ — the mean number of source events for which signal was declared in 90% or better of 400 trials with a cut on $F = .15$ — at 21 grid points in the Northern Hemisphere. Exact numbers and locations of gridpoints are given in Table 1.The systematic uncertainty in the calculation of $N_{.15}$, due to uncertainties in the size of the error ellipses, is ≤ 1 event.
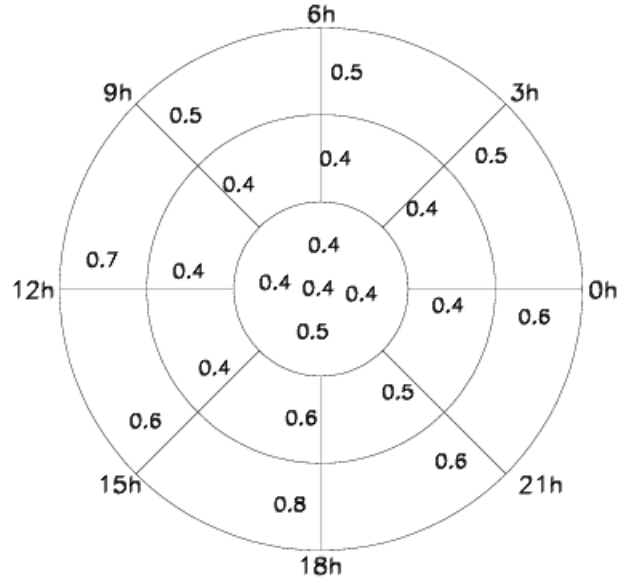
Fig. 16. 90% c.l. Flux Upper Limit (cosmic rays/km^{2}yr) at 21 grid points in the Northern Hemisphere. Flux upper limit is calculated by dividing $N_{.15}$ by the exposure at each grid point. Exact numbers and locations of gridpoints are given in Table 1.

DEC (deg)	RA (hours)	$N_{.33}$	$N_{.15}$	Exposure (km^2yr)	Sensitivity (cosmic rays/km²yr)	Upper Limit (cosmic rays/km²yr)
15°	2.5 hrs	23	16	34.2	.7	.5
	5.5 hrs	24	19	36.6	.7	.5
	8.5 hrs	22	16	34.3	.6	.5
	11.5 hrs	20	16	24.5	.8	.7
	14.5 hrs	18	14	21.9	.8	.6
	17.5 hrs	18	13	16.7	1.1	.8
	20.5 hrs	17	13	21.1	.8	.6
	23.5 hrs	21	16	26.7	.8	.6
45°	2.5 hrs	26	20	49.7	.5	.4
	5.5 hrs	29	22	56.6	.5	.4
	8.5 hrs	25	20	48.5	.5	.4
	11.5 hrs	24	18	41.2	.6	.4
	14.5 hrs	21	15	33.5	.6	.4
	17.5 hrs	21	16	24.9	.8	.6
	20.5 hrs	21	16	30.3	.7	.5
	23.5 hrs	24	18	41.5	.6	.4
75°	5.5 hrs	29	21	59.8	.5	.4
	11.5 hrs	28	21	50.5	.6	.4
	17.5 hrs	26	19	38.6	.7	.5
	23.5 hrs	26	20	47.2	.6	.4
90°	N/A	31	23	53.8	.6	.4

Table 1

 Locations of gridpoints, threshold signal strengths $N_{.33}$ and $N_{.15}$, exposures (with uncertainty 5%, primarily from Monte Carlo statistics), detector flux sensitivity, and 90% confidence level flux upper limits, for cosmic rays with energy exceeding $10^{18.5}$ eV.

7 Conclusions

We have conducted a search for point-like excesses in the arrival direction of ultra–high energy cosmic rays with energy exceeding $10^{18.5}$ eV in the northern hemisphere. We place an upper limit of 0.8 cosmic rays/(km^2 yr) (90% c.l.) on the flux from such sources across the entire sky and place more stringent limits as a function of position. We also determine sensitivity as a function of position in the sky. The HiRes–I monocular data is thus consistent with the null hypothesis for point-like excesses of neutral primary cosmic rays in this energy range.

References

[1] R. Abbasi *et al.*, Astroparticle Physics **21** (2004) 111.

[2] N. Hayashida *et al.*, Astroparticle Physics **10** (1999) 303.

[3] G.L. Cassiday *et al.*, Phys. Rev. Lett. **62** (1989) 383.

[4] M. Teshima *et al.*, Phys. Rev. Lett. **64** (1990) 1628.

[5] M. A. Lawrence *et al.*, Phys. Rev. Lett. **63** (1989) 1121.

[6] A. Borione *et al.*, Phys. Rev. **D55** (1997) 1714.

[7] T. Doi *et al.* Proc. 24th ICRC (Rome) **2** (1995) 804.

[8] L. M. Widrow, Rev. Mod. Phys. **74** (2003) 775.

[9] R.U. Abbasi *et al.*, Phys. Rev. Lett. **92** (2004) 151101.

[10] D. J. Bird *et al.*, Proc. 23rd ICRC, Calgary **2** (1993) 38.

[11] D. J. Bird *et al.*, Astrophysical Journal **424** (1994) 491.

[12] G.J. Feldman and R.D. Cousins, Phys. Rev. D, Vol **57** Number 7 (1998) 3873.

[13] B. Stokes, Ph.D. Thesis, University of Utah (2005).